Potential Contours in Ion Focusing Hall Thruster

Kunning G. Xu[1], Hoang Dao[2] and Mitchell L.R. Walker[3]

High-Power Electric Propulsion Laboratory, Georgia Institute of Technology, Atlanta, GA 30332 USA

The Embedded Electrode Hall Effect Thruster is a modified 10 kW T-220HT with embedded graphite electrodes within the channel wall to study ion focusing for improved thrust-to-power ratio. Previous experiments with the thruster have demonstrated increased performance on xenon with biased electrodes caused by increases in ion energy, propellant efficiency, and a reduction in the plume divergence angle. In this paper, the in-channel plasma potential is experimentally mapped with emissive probes to determine the effect of the cusp-magnetic fields and wall electrodes on the plasma. The resultant potential contours indicate a significant compression in the potential field and acceleration region by 4 – 10 cm when the electrodes are biased to 30 V and creation of domed high-potential regions that are responsible for focusing electric fields.

Nomenclature

A	=	Wall sheath area
A_c	=	Channel cross-section area
D_r	=	Channel diameter ratio, outer/inner diameter
e	=	Electron charge
I_b	=	Ion beam current
I_d	=	Discharge current
I_S	=	Sheath current
$J_{e,i}$	=	Electron and ion current density
k_B	=	Boltzmann's constant
k_r	=	Election-ion recombination constant
L_C	=	Channel length from anode to exit plane
M	=	Ion mass
m_i, m_e, m_n	=	Ion, electron, and neutral particle mass
n_i, n_e, n_n	=	Ion, electron, and neutral number density
n_o	=	Bulk plasma density
T_e	=	Electron temperature
T_n	=	Neutral temperature
V_f	=	Floating potential
V_p	=	Plasma potential
v_e	=	electron velocity
v_i	=	Ion velocity
v_n	=	Neutral velocity
v_{th}	=	Thermal velocity
α	=	Electron-ion recombination constant
η_b	=	Beam efficiency
λ_D	=	Debye length
λ_i	=	Ionization mean free path
σ_i	=	Collision cross-section
v_e	=	Electron-ion collisions frequency
Ω_e	=	Electron Hall parameter
Φ	=	Potential

---

[1] Graduate Student, Aerospace Engineering, 270 Ferst Dr NW, Full Member AIAA.
[2] Undergraduate Student, Aerospace Engineering, 270 Ferst Dr NW, Student Member AIAA.
[3] Associate Professor, Aerospace Engineering, 270 Ferst Dr NW, Associate Fellow AIAA.

American Institute of Aeronautics and Astronautics

I.   Introduction

Hall effect thrusters (HET) produce thrust through the electrostatic acceleration of ions produced via collisional ionization. Ions are accelerated by the electric field generated between the cathode and anode. The ion population has a spread of velocity vectors, some terminating in the discharge channel walls. These ions that strike the channel wall are neutralized and leave the thruster providing less thrust that a fully accelerated ion. Reduction of ion loss due to wall-neutralization is one method to increase the ion density and performance of HETs. One method to reduce wall collisions is shaping the potential field, and thus the electric field, within the discharge channel. Electric field lines that converge along the channel centerline would both reduce ion wall losses and beam divergence.

In order to control the potential field, secondary electrodes are embedded along the channel wall and biased above anode potential to affect the in-channel potential distribution. The thruster magnetic field design produces a non-radial topography. The magnetic field helps to generate a focused electric field due to the observed property of thermalized potential, where magnetic field lines approximate equipotential lines.[1, 2] Previous work have shown that biasing the electrodes 10 or 30 V above anode potential increases the thrust, specific impulse, thrust-to-power ratio, and anode efficiency.[3] In that work, plume characterization of the thruster operating with biased electrodes, shows a decrease in the plume divergence angle, an increase propellant efficiency, and an increase in ion energy. In order to understand how the electrodes affect the plasma, in-channel measurements are made.

This paper presents the in-channel potential measurements of a HET with embedded wall electrodes. Section II presents the experimental setup and the reviews the modifications to the thruster. Section III presents a basic calculation of ionization and wall losses based on analytical equations. Section IV presents the measured potential maps of the in-channel area for the conditions tested. Finally Section V discusses the results and implications.

II.   Experimental Setup

A. Hall Thruster

All experiments are performed on a modified Pratt & Whitney Rocketdyne T-220HT HET. Extensive testing has mapped the performance of the thruster over a power range of 2-22 kW at discharge voltages of 200-600 V.[4] The T-220HT has a mean channel diameter of 188 mm, channel depth of 65 mm, and nominal power rating of 10 kW. An Electric Propulsion Laboratory 375 series cathode is located at the 12 o'clock position on the thruster and aligned with the local magnetic field. The cathode orifice is located approximately 30 mm downstream from the front face of the thruster. The cathode flow rate is set at 1 mg/s for all cases investigated. The discharge channel of the thruster is made of M26 grade boron nitride (BN). A more detailed description of the T-220HT and its characteristics can be found in Reference 4.

The T-220HT HET discharge supply is a Magna-Power 45 kW DC power supply and all electrical connections enter the chamber through separate feedthroughs. The thruster discharge supply is connected to a filter consisting of a 1.3 Ω resistor in series and 95 μF capacitor in parallel with the discharge supply. The filter acts as a low-pass filter, which prevent oscillations in the current over 1.4 kHz from reaching the discharge supply. High-purity (99.995%) xenon propellant is supplied to the thruster via stainless steel lines. MKS 1179A mass flow controllers meter the propellant flow to the cathode and anode. The flow controllers are calibrated by measuring gas pressure and temperature as a function of time in a known control volume.

B. Magnet Field Design

The magnetic field topography of the T-220HT was redesigned to include the addition of a pair of cusp-magnetic fields along the channel wall to shield the electrodes from strong electron current. In a standard HET magnetic field, radial magnetic field lines would terminate on the electrodes, sinking magnetized electrons into the electrode circuit. The goal of the cusp fields is to reduce the electron current to the electrodes and any negative impact on the thruster performance.

The static magnetic field is simulated with the commercial software MagNet by Infolytica. shows the final magnetic field topography for the EEHET. The anode and electrodes are labeled. The designed magnetic field has a high concavity for the majority of the channel length. Following the common assumption that magnetic field lines are equipotential contours,[1] this will allow an enhanced focusing of the electric field toward centerline. The field also provides ample coverage of the electrodes with cusp fields. The cusp field strength is strong enough to magnetize 25 eV electrons, an average electron temperature seen in HETs of this size.[5, 6]
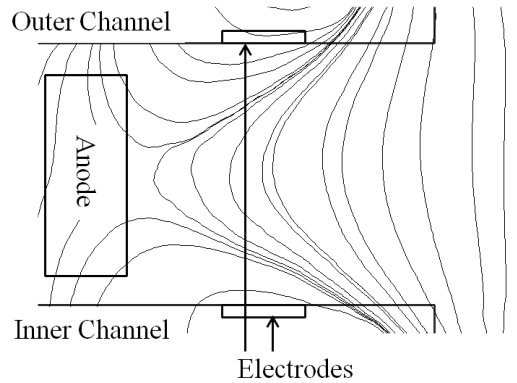
Figure 1. Location of the magnetic field structure for the EEHET with respect to the electrodes. Cusp-magnetic fields are generated to cover the electrodes while retaining a plasma lens near the discharge channel exit plane.

C. Electrodes

The ring electrodes used in the EEHET are machined from isomolded, super fine grain graphite plates. The pair of rings is designed to sit within the BN channel wall to preserve a smooth, constant radius channel surface. BN material is removed from the channel to permit the addition of the rings. Additional BN rings are used to fill in any space between the electrodes and the channel exit to maintain constant geometry. The electrode placement is based on three main considerations: cusp-magnetic field placement, Hall current shorting, and wall ion number density. A dual requirement of a radial plasma lens near the exit for high performance and cusp fields for electrodes shielding means the cusp fields must be placed upstream of the channel exit. Cusp fields placed near the channel exit would cause large axial magnetic fields which could interfere with thruster operation. The second factor that contributes to an upstream placement of the electrodes is the presence of the electron Hall current near the magnetic field peak.[5] The Hall current is comprised of the high-energy cathode electrons that cause ionization of propellant. A biased electrode, especially a positive one, place within the Hall current would collect electrons and effectively short the Hall current. This would prevent the thruster from operating when the electrodes are biased. Figure 2 shows the radial magnetic field profile for the T-220HT and the average location of the exit plane and electrodes.

These two factors indicate an upstream placement of the electrodes away from the channel exit. The last consideration, the ion wall density, actually says the opposite. This work is interested in reducing ion-wall collisions, thus it is logical to place the electrodes in areas with a high rate of ion wall collisions. The majority of wall collisions occur near the exit plane of the thruster where the electric field begins to diverge. This behavior appears in both models[7] and experiments[8]. Shastry calculated the ion density at the channel wall using wall-mounted Langmuir probes and compared it to simulations results from HPHall-2. Both results show the density peaks around $0.15 \, L_C$ from the exit plane, where L_C is the channel length from the exit plane to the anode, and drops quickly to zero past $0.5 \, L_C$.[8] This would suggest the electrodes should be placed at $0.15 \, L_C$. However this location would cause the cusp-magnetic fields to interfere with the exit magnetic field as mentioned. Thus, the compromise was made to place the electrode leading edge at $0.5 \, L_C$. At this location the electric field should still affect some of the near-wall ions and allow a plasma lens near the discharge channel exit plane.
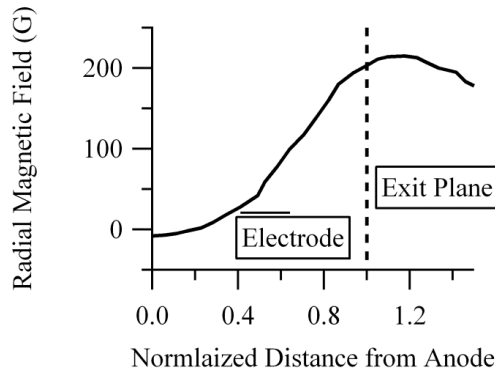
American Institute of Aeronautics and Astronautics

Figure 2. Electrode placement relative to radial magnetic field and channel exit.

The embedded electrodes in this work physically are 10-mm wide and 1.6-mm thick. They are located the same axial distance from the anode, which puts them about 37 mm from the channel exit plane. Figure 3 shows the electrical schematic for the added electrodes. The key point to note is the electrodes are biased above the anode, thus the electrode supply only needs to provide a few volts of potential, and at zero potential on the electrode power supply, the electrodes would be at anode potential.
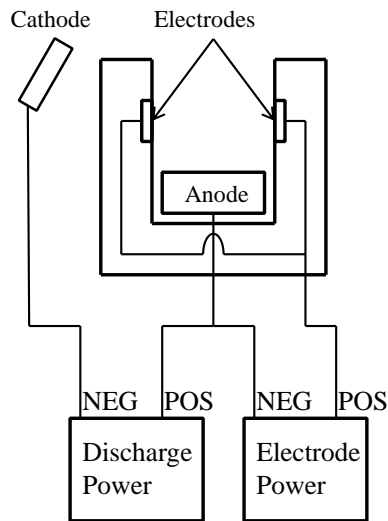
Figure 3. EEHET electrode wiring diagram.

D. In-Channel Measurement Setup

Measurement of the discharge plasma requires high speed interrogation to prevent probe damage and perturbations to the plasma. Inside the discharge of a HET, the high-energy particles sputter and ablate probe materials. The deposition of probe materials can affect local plasma parameter and perturb thruster operation. Thus, for accuracy and probe survival, a short residence time (<150 ms)[5] is necessary. To that end a High-Speed Axial Reciprocating Probe (HARP) system is used. An Aerotech linear motor is mounted on an aluminum frame with a stainless steel probe arm. Graphite plates protect the motor from thruster discharges. The system is capable of speeds up to 3 m/s, with a residence time in the plasma on the average of 100 ms. Figure 4 shows the HARP system in the chamber ready for use on the EEHET. A miniature emissive probe is mounted on the HARP arm.
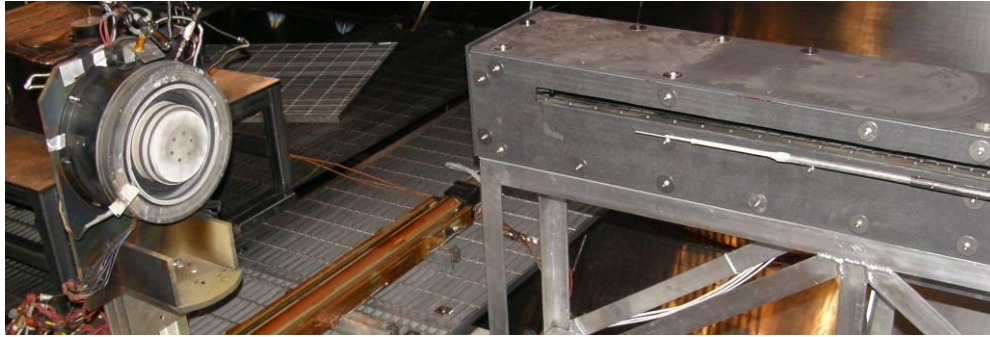
4
American Institute of Aeronautics and Astronautics

Figure 4. In-channel measurement setup showing the thruster on the left and the HARP with emissive probe on the right.

To measure the plasma potential within the short residence time of the HARP, a miniature floating emissive probe is used for its instantaneous measurement. The emissive probe used in this study is based on the ones used by Reid.[6] A 0.13-mm diameter thoriated tungsten wire filament is inserted into a 1.5 mm diameter double bored alumina tube. The filament loop has a radius of approximately 1 mm. Current is applied to the filament which generates thermionic electron emission. The emitted electrons neutralize the sheath that forms around the filament and allows the probe to float at the local plasma potential.

The channel plasma and floating potential are mapped for an area 26 mm wide by 50 mm long. The measurement region extends from a few millimeter past the channel exit plane to within ~6 mm of the anode surface. Figure 5 shows a schematic of the area mapped with the probe and the locations of the measurements. The measurement locations are spaced 5 mm ± 1 um axially. The radial measurements have decreasing steps from 4 to 1 mm (± 5 um) in order to provide better resolution of changes near the channel surfaces. Prior to data collection, the emissive probe heating current versus measured potential both in and out of the channel is plotted to ensure sufficient emission.
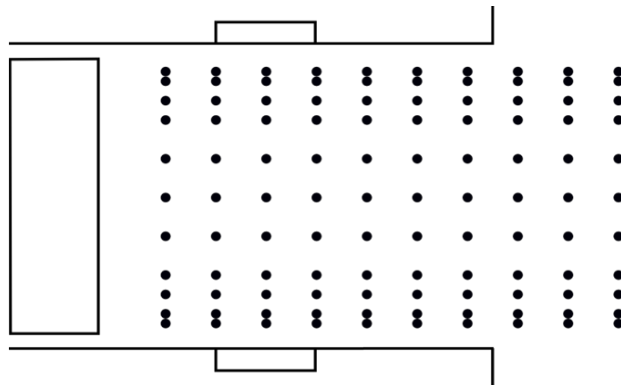

Figure 5. In-channel points mapped with the miniature emissive probe.

E. Vacuum Facility

All experiments are performed in the Vacuum Test Facility 2 (VTF-2) shown in Figure 6. VTF-2 is 9.2 meters long and 4.9 meters in diameter. It is pumped to rough vacuum with one 3800 CFM blower and one 495 CFM rotary-vane pump. Ten liquid nitrogen cooled CVI TMI re-entrant cryopumps with a combined pumping speed of 350,000 l/s on xenon bring the chamber to a base pressure of 5×10^{-9} Torr. A Stirling Cryogenics SPC-8 RL Special Closed-Looped Nitrogen Liquefaction System supplies liquid nitrogen to the cryopump shrouds. MKS 1179A mass flow controllers meter the propellant and a constant volume calibration system is used to calibration the mass flow rate. Two ionization gauges, Varian 571 and UHV-24, are mounted on either side of the chamber.
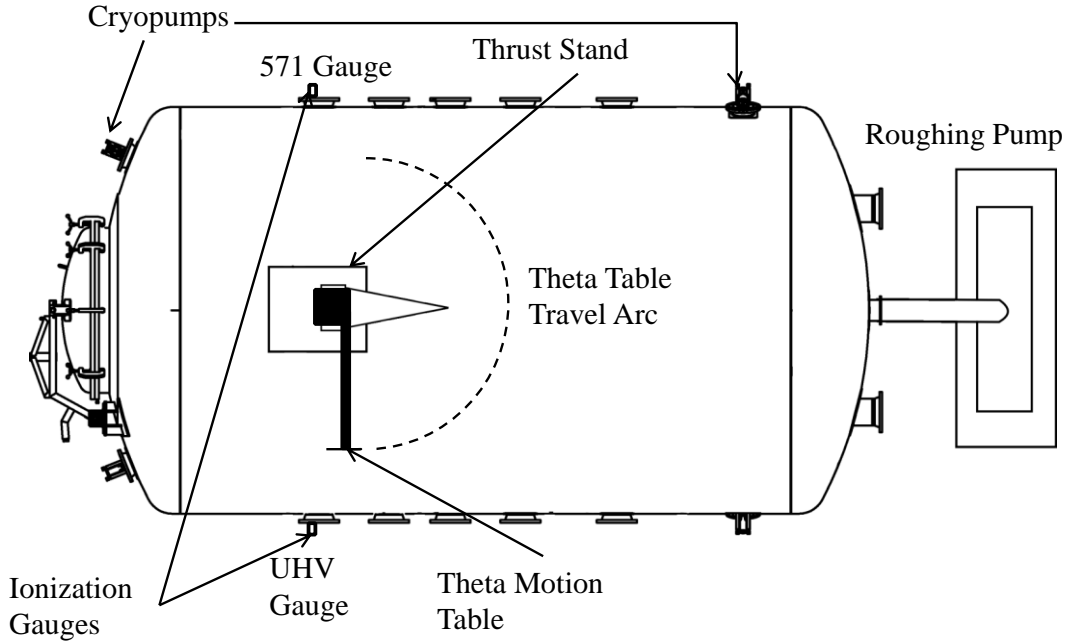
5
American Institute of Aeronautics and Astronautics

Figure 6. Schematic of VTF-2 (not to scale).

III.   Ionization and Recombination

The stated goal of this work is to increase HET performance by reducing ion losses, specifically ion-wall neutralization. It is thus prudent to consider the ion sources and sinks present in HETs to determine the percentage of total ions lost to wall neutralization. There are two primary sources of ion loses, wall and particle collisions. Both will be described and their contributions to the total ion population analyzed.

A. Ionization

The ionization process in HETs is purely collisional. Electrons emitted from the cathode obtain energy from the electric field and collide with neutral atoms to create ions. The production rate of ions is given by the rate equation

$$\frac{dn_i}{dt} = n_n n_e \langle \sigma_i v_e \rangle \tag{1}$$

where n_i and n_n are the ion and neutral particle densities respectively, σ_i the ionization cross-section, and v_e the electron velocity. The term in the brackets is the ionization reaction rate constant, which is the ionization cross-section averaged over the electron velocity distribution function. The values for the ionization rate constant have been tabulated for multiple temperatures. Goebel[9] presents tabulated xenon ionization constants for electron temperatures up to 10 eV, and curve fits for larger values of T_e. His calculations are used here.

The electron number density, which from the quasi-neutral assumption is equal to the ion number density, can be calculated from the ion beam exiting the thruster from

$$n_e = \frac{I_b}{e v_b A_c} = \frac{\eta_b I_d}{e A_c \sqrt{\frac{2\eta_b e V_d}{M}}} \tag{2}$$

where I_b is the measured ion beam current, e is the electron charge, A_c is the channel area, η_b is the beam efficiency which is equal to the beam current divided by discharge current (I_b/I_d), and M is the ion mass (2.18 x 10^{-25} kg for xenon). The measured beam current from previous data varied from 6.9 to 8.2 A for a 9 A discharge current on the anode.[3] The difference between the ion current exiting the thruster and the electrical discharge current seen by the anode is due to ion losses and the electron leakage current.

American Institute of Aeronautics and Astronautics

The discharge current consists of two primary sets of electrons: ionization electrons and cathode electrons. The dominant source of the discharge current comes from the ionization of propellant where the electrons removed from the neutral atoms are collected by the anode. Cathode electrons that slowly make their way across the magnetic field to the anode also make a small contribution to the discharge current. The cathode electrons are caught on the strong magnetic field, but every collision causes the electrons to lose energy and jump to a weaker magnetic field and eventually reached the anode. This is called the leakage current. Thus only a portion of the discharge current is from ions. Taking an average I_b of 7.6 A for an I_d of 9 A at a discharge voltage of 200 V yields an electron number density of 1.6 x 10^{17} m^{-3}. This is on the low end of the in-channel measured and simulated electron density from the literature, but sufficient for our purposes.[5, 7, 10, 11]

It is interesting to note that Eq. (2) has very little variation in the electron density with the three variables: discharge current, discharge voltage, and beam efficiency. There is a linear variation due to beam current, I_d, if voltage and beam efficiency are held constant. However HETs typically operate over small current ranges, say 10 – 40 A, thus the effect of current on density is small.

The effects of voltage and beam efficiency are even smaller. For a voltage range of 100 to 1000 V and efficiency of 0.1 to 1, both only increase the density by a maximum of 3.16 times, if the other parameters are held constant. In reality the voltage, current, and beam efficiency are tied together. Assuming a constant propellant supply, increased voltage creates more energetic electrons with energy approximately 1/10th the voltage, which results in higher beam current and higher beam efficiency. The three variables will thus tend to cancel one another and make the overall change in electron density even smaller. This can also be seen from measured data of in-channel plasma density.[5, 6, 10] The point of this detour is to show the plasma density is a rather stable value in HETs for a large range of operating conditions.

The neutral density is typically two orders of magnitude larger than the plasma density, so will be taken as 1 x 10^{19} m^{-3}.[6, 10, 12] The electron temperature in the ionization region is usually on the order of 20 eV or more. A value of 25 eV will be assumed for this analysis. This falls within the range measured for this thruster as will be shown later. The resulting ion production rate constant is thus 2.14 x 10^{23} m^{-3}s^{-1}.

The ionization process occurs within a relatively small volume of the discharge channel upstream of the magnetic field peak.[6, 9, 10] This axial distance is on the order of the characteristic ionization mean free path (MFP) λ_i.

$$\lambda_i = \frac{v_n}{n_e \langle \sigma_i v_e \rangle} \tag{3}$$

Here v_n is the neutral particle velocity which can be calculated from the mean 3-D thermal velocity,

$$v_n = v_{th} = \sqrt{\frac{8 k_b T_n}{\pi m_n}} \tag{4}$$

where k_b is the Boltzmann constant, T_n is the neutral particle temperature, and m_n the neutral mass. The neutral temperature can vary greatly depending on operating conditions. Huang measured the neutral temperature inside a HET channel with laser-induced fluorescence and showed the temperature can vary from 600 – 1600 K.[13] The operating conditions in this work correspond to an average of 800 K based on his results. This gives a neutral velocity of 357.5 m/s. The resulting ionization MFP is thus 1.67 cm. Multiplying by the channel area, the total ion production rate is 6.76 x 10^{19} s^{-1}, which is an ion current of 10.8 A. This is larger than the assumed beam or discharge current, but acceptable for this analysis.

Combining Eq. (1) – (4), one can calculate the ion current from ionization as shown in Eq. (5). This ion current is independent of the electron density and the electron temperature. The combined current equation only depends on the neutral temperature and density.

$$I_i = e A_c \frac{d n_i}{dt} \lambda_i = e A_c (n_n n_e \langle \sigma_i v_e \rangle) \left(\frac{v_n}{n_e \langle \sigma_i v_e \rangle} \right)$$

$$= e A_c n_n v_n = e A_c n_n \sqrt{\frac{8 k_b T}{\pi m}} \tag{5}$$

Eq. (5) makes sense since an increased ionization rate means a decreased ionization MFP, with a net result being a small increase in ion production. An increase in the neutral density means increased propellant flow rate and thus

increased current. A larger channel area can also cause increased ion current, assuming the propellant flow rate is increased to maintain the neutral density. So for high ion current, a large thruster with high flow rate is desirable.

B. Electron-Ion Recombination

Electron-ion recombination will decrease the number of ions available for thrust, if the ions recombine prior to exiting the thruster. So for concerns of net thrust loss due to electron-ion recombination, only the ionization and acceleration regions need to be considered. The electron-ion recombination rate equation (assuming electrons are the dominant third-body) is

$$\frac{dn_i}{dt} = -k_r n_e{}^2 n_i = -\alpha n_e n_i \tag{6}$$

where k_r is the recombination rate constant, which can be calculated as α from [14]

$$\alpha = 1.09 \; x \; 10^{-20} n_e T^{-\frac{9}{2}} \; m^3/s. \tag{7}$$

Using the density and temperature values from the previous section, the electron-ion recombination rate constant is 1.17 x 10^7 m^{-3}s^{-1}. The acceleration region has a length of $3 - 5$ cm as will be shown in Section V-A. Taking an average length of 4 cm, combined with the ionization mean free path and channel area gives the ions lost to electron recombination as 1.26 x 10^4 s^{-1}, which is a current of 2 x 10^{-15} A. This is a miniscule amount of ions lost compared to the 10.8 A of ions produced. The recombination current is strongly dependent on plasma density and electron temperature. However even trying to maximize the recombination with a very low temperature of 5 eV and high density of 5 x 10^{19} m^{-3}, the recombination current is only 6 x 10^{-5} A; thus electron-ion recombination has a negligible impact on thruster performance.

C. Wall Losses

Ion-wall losses result from ion collisions with the channel wall. The quasi-neutral property of the plasma means on a macroscopic level, the plasma is free of electric fields, thus any ions that reach the wall are due to random thermal motions. At the wall, a thin plasma sheath region exists where quasi-neutrality breaks down and electric fields can exist. The sheath exists due to the different fluxes between electrons and ions. The ratio of electron to ion current flux, assuming quasi-neutrality, is

$$\frac{J_e}{J_i} = \frac{n_e e v_e}{n_i e v_i} = \frac{v_e}{v_i} \tag{8}$$

where J is the current density, e is the charge on the particle, and v is the particle velocity. The i and e subscripts correspond to ions and electrons respectively. The average 1-D particle thermal velocity is

$$v_{th} = \sqrt{\frac{2k_b T}{\pi m}} \tag{9}$$

If the ion and electron temperatures are assumed equal, then the current density ratio is proportional to the square root of the mass ratio.

$$\frac{J_e}{J_i} = \frac{v_e}{v_i} = \sqrt{\frac{m_i}{m_e}} \tag{10}$$

Ions are much heavier than electrons, for example the square root of the mass ratio for xenon is 491. This means the electron flux is much larger, and electrons will strike the wall before ions. This causes the wall potential to decrease and become negatively charged, which attracts ions and repels electrons. This decreases the electron flux to the surface. The wall potential and sheath stabilizes when the ion and electron flux at the sheath edge are equal. Inside the sheath, the potential decreases from the plasma potential to the wall potential. The sheath potential drop accelerates ions in the sheath toward the wall. The ion flux to the wall can thus be assumed equal to the ion density at the sheath edge if the sheath is assumed collisionless.

The plasma density at the sheath edge is 60.6% of the plasma density in the plasma far away from the sheath. This arises from the Bohm sheath criterion, which states that in order to have a monotonically decreasing potential

American Institute of Aeronautics and Astronautics

in the sheath, ions must fall through a potential of at least $T_e/2$ before entering the sheath. This expression can be written as

$$\Phi_o > \frac{k_b T_e}{2e} \qquad (11)$$

where Φ_o is the potential drop. This condition can be expressed in terms of a velocity from the electric to kinetic energy balance $e\Phi = 1/2\, mv^2$:

$$v_i = \sqrt{\frac{2e\Phi}{m_i}} \qquad (12)$$

The resulting velocity

$$v_i \geq \sqrt{\frac{k_b T_e}{m_i}} \qquad (13)$$

is known as the Bohm velocity, or ion acoustic velocity when entering a sheath. Combining Eq. (11)   with   the Boltzmann equation for electrons,

$$n_e = n_o exp\left(\frac{e\Phi_o}{k_b T_e}\right) \qquad (14)$$

where n_o is the plasma density far away from the sheath, gives

$$n_e = n_o exp\left[\left(\frac{e}{k_b T_e}\right)\left(\frac{-k_b T_e}{2e}\right)\right]$$

$$= 0.606 n_o \;. \qquad (15)$$

The negative sign in Eq. (15) comes from the potential drop from the bulk plasma to the sheath edge. Knowing the plasma density, and thus ion density at the sheath edge, it is possible calculate a value for the current loss to the wall. The assumption made here is all ions that enter the sheath strike the wall and become neutralized. This is a valid assumption as the sheath is very thin, typically less than 1 mm, and the potential profile within the sheath causes ion acceleration toward the surface. Thus, the sheath ion current density can be written as

$$J_i = 0.6 n_o e v_i = 0.6 n_o e \sqrt{\frac{k_b T_e}{m_i}} \;. \qquad (16)$$

Eq. (16) can also be written in terms of a sheath current, I_S, for a sheath area A.

$$I_S = 0.6 n_o e A \sqrt{\frac{k_b T_e}{m_i}} \qquad (17)$$

Using the plasma density of 1.6×10^{17} m^{-3} calculated in Section III-A, and half the channel surface area for the reasons mentioned in Section II-C (there are no ions in the near anode region), the ion current lost to the walls is estimated to be 1.37 A. This is almost 13% of the total produced ion current, which means reducing this loss of ions to the walls could provide a significant increase in the thruster performance.

It should be mentioned that the surface area assumed here is based on the assumption of no ions at the wall upstream of 0.5 L_C. This assumption was based on data of another thruster, the H6 from the University of Michigan.[8] The H6 and the T-220HT are similar in size, power, and design, thus the correlation is made with a reasonable level of confidence. In general, the location of wall ions is dictated by factors such as the placement of the ionization zone and magnetic field, which will be different for different thrusters. Another method to define the beginning of the ionization region, and thus the beginning of the wall loss region, is to consider the location of the 12 eV electron temperature contour. The first ionization energy of xenon is 12.13 eV, and thus the 12 eV contour can be assumed as

the start of the ionization region. As will be shown later in Section V-B, the 12 eV contour in this work roughly corresponds to half the channel length, thus the half surface area approximation used above is reasonable.

The expression for ions lost to the wall can be simplified by combining the result of Eqs. (5) and (17):

$$\frac{I_S}{I_i} = \frac{n_o e A \sqrt{\frac{k_b T_e}{m_i}}}{e A_c n_n \sqrt{\frac{8 k_b T_n}{\pi m_n}}} = \frac{0.6 n_o A}{n_n A_c} \sqrt{\frac{\pi T_e}{8 T_n}}$$

$$= 0.626 \frac{n_o A}{n_n A_c} \sqrt{\frac{T_e}{T_n}} \tag{18}$$

Here, the neutral mass is taken to be equal to the ion mass. The neutral density is generally two orders of magnitude larger than the plasma density as mentioned before, thus the ratio n_o/n_n is around $0.01 - 0.02$. The square root of the temperature ratio also tends to stay relatively constant around $10 - 12$. This is because a higher electron temperature causes heating of the anode and channel walls, which subsequently heats the neutral propellant. Without external cooling, the neutral temperature should track the electron temperature relatively well. Thus, the only major factor in the fraction of ions lost to the walls is the dimensions of the thruster channel. The term A/A_c can be broken down into considerations of channel length and diameter.

$$\frac{A}{A_c} = \frac{\pi L_C}{2}(OD + ID) \Big/ \frac{\pi}{4}(OD^2 - ID^2)$$

$$= 2 L_C \frac{OD + ID}{OD^2 - ID^2}$$

$$= \frac{2 L_C}{OD - ID} = \frac{2 L_C}{D_r - 1} \tag{19}$$

Here OD and ID refer to the outer and inner diameter of the discharge channel, and D_r is the ratio of outer to inner wall diameter. The channel surface area is taken as half the total surface area as done previously. Combining this with Eq. (18) and replacing the density and temperature ratios with constants 0.015 and 11 respectively gives:

$$\frac{I_S}{I_i} = 0.224 \frac{L_C}{D_r - 1} \tag{20}$$

This suggests that the fraction of ions lost to the wall can be reduced by designing thrusters with shorter channels and larger channel area. The latter occurs because an increase in outer diameter or decrease in inner diameter causes the channel exit area to increase faster than the surface area. Thus ion production increases faster than wall losses. Using the dimensions for the T220-HT, Eq. (20) under predicts the percent ion-wall losses by 20% compared to the loss calculated using actual plasma properties. It is useful, however, as an approximation for wall losses. A more thorough analysis of the particle interactions, such as how neutral temperature scales with electron temperature, or how neutral density relates to ionization rate and channel dimension, would give a more accurate prediction of ion-wall loss.

Many assumptions were made for this analysis. The actual physics inside the thruster are more complicated than these equations reflect. Nonetheless, the results show that ion-wall neutralizations are a significant portion of the total ions produces, and much greater than ions lost through electron-ion recombination.

IV.   Results

The thruster is tested at a discharge voltage of 150 V and a discharge current of 9 A on xenon propellant. This voltage was chosen because performance data showed significant improvements at this voltage,[3] in addition the lower power increases probe survivability. The thruster is run in constant current mode by varying the anode mass flow to maintain a discharge current of 9 ± 0.1 A. The anode mass flow rate was varied from 10.02 to 10.36 mg/s. The magnetic field is also kept constant for all tests. Thus, the currents are not optimized for each operating point. This is done in order to reduce the impact of variable magnetic field structure between each operating condition.

The thruster is tested at three electrode conditions: Floating, 10 V_e, and 30 V_e, where the subscript denotes electrode. The Floating case has the electrodes installed but electrically isolated from the power supply. In the 10

and 30 V_e conditions, 10 or 30 additional volts above anode potential are placed on the electrodes via their power supplies. For example, at 150 V on the anode and 10 V_e, the electrodes are actually at 160 V with respect to the cathode. Figure 7 shows the plasma potential contours for xenon at discharge voltage of 150 V and a discharge current of 9 A. The cathode-to-ground voltage is relatively constant at -20 V. The Floating condition shows a potential distribution with a high gradient near the channel exit that defines the ionization/acceleration region. The contours are convex and create a diverging electric field near the exit. The diverging electric field will give ions increased radial velocities and cause increased plume divergence angle. Near the anode and electrodes, the potential is relatively flat and surrounds the anode. The potential ranges from 65 to 130 V.

With powered electrodes, there are two main changes to the potential contours. The first is a division of the high potential regions at the upstream end of the channel near the electrodes. At 30 V_e, and somewhat at 10 V_e, that the high potential region near the anode and electrodes split into two separate areas with a lower potential area in between. The domed areas of high potential conform to the cusp-shaped magnetic field regions to a first order as shown in Figure 8. The domed potentials will generate electric fields in the back of the channel pointed toward channel centerline. These fields in turn will focus ions.

The second main change that can be seen in the potential measurements is the increase in potential range. When discharge voltage is increased, the potential contours typically experience a similar increase in maximum potential. This is true in the 30 V_e case, but not so at 10 V_e. At 10 V_e, the maximum potential increased by less than two volts over the Floating case. The high potential region is expanded to cover a larger area though. At 30 V_e, the maximum potential increased by 30 V over the Floating case. At this condition, the maximum potential becomes dictated by the electrodes instead of the anode.
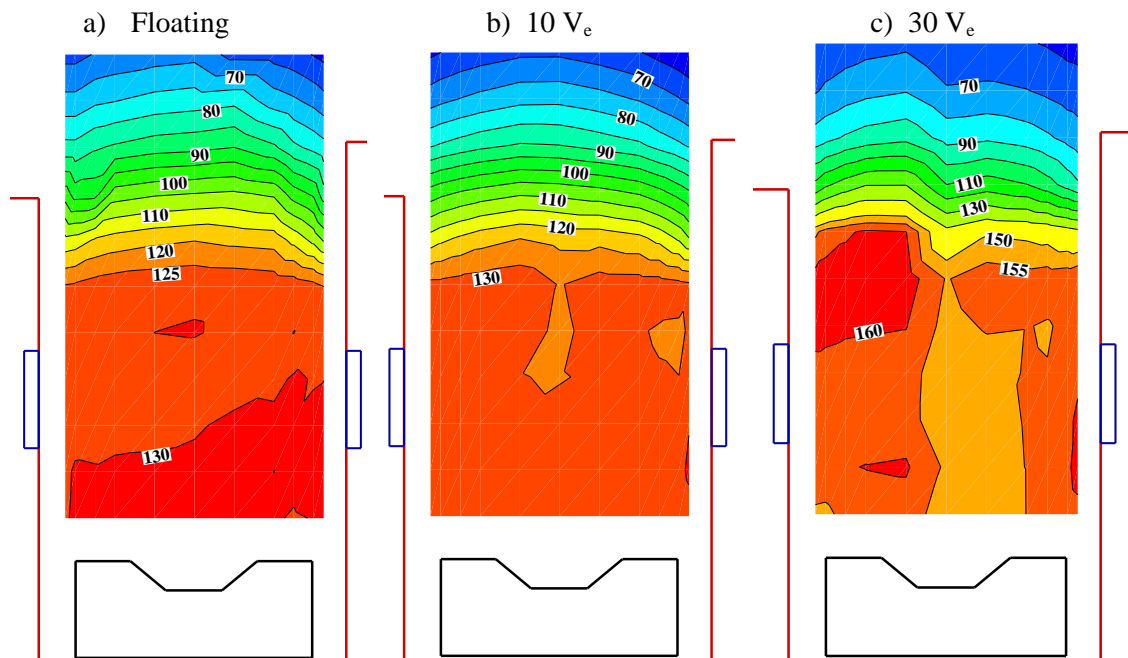

Figure 7. In-channel plasma potential map for 150 V anode discharge with Floating, 10, and 30 V_e electrode conditions. The values denote the potential, in volts, of each contour.
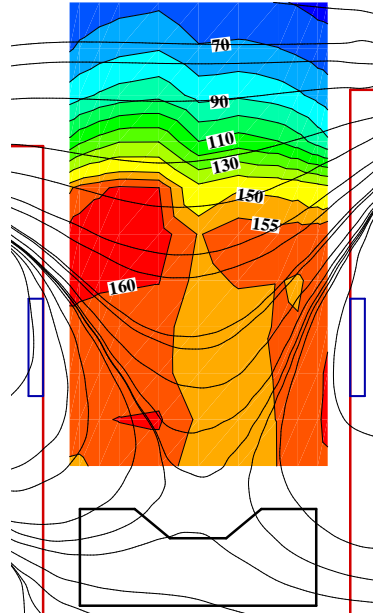
American Institute of Aeronautics and Astronautics

Figure 8. 150 V floating and 30 V$_e$ case on xenon with magnetic field overlay.

V.   Discussion

Past performance and plume measurements of the EEHET showed increased performance with the electrodes.[3] Figure 9 shows the thrust and thrust-to-power (T/P) ratio data obtained with xenon propellant at 9 A discharge. The electrodes increase the thrust at both 10 and 30 V$_e$, however the T/P ratio is only improved at 10 V$_e$. Mathematically this is caused by an increase in the electrode current offsetting any thrust gains. Physically the cause of the increase in T/P ratio is not known, and is one purpose of the in-channel measurements.
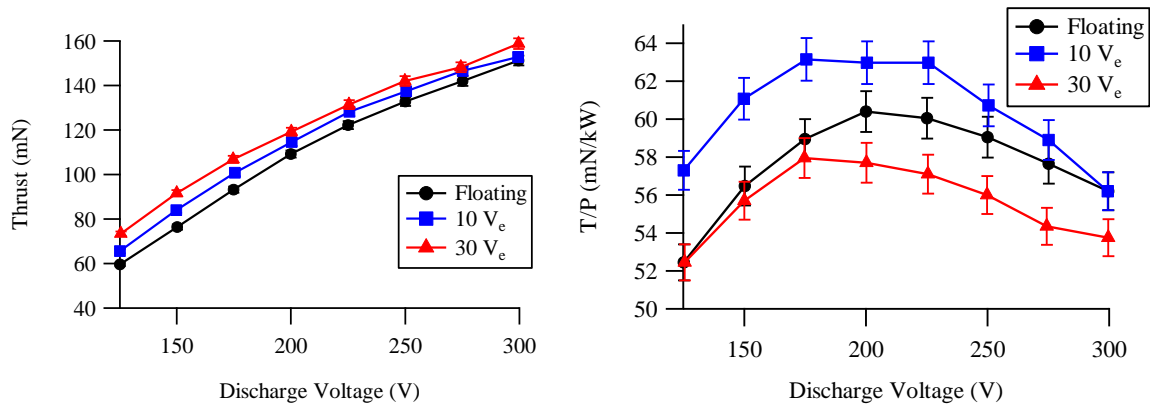

Figure 9. Thrust and thrust-to-power ratio for the EEHET on xenon at 9 A.

In addition to different T/P ratio changes, the two biased electrode levels caused different changes in the ion energy. Figure 10 shows the most probably ion energy (± 6.5 V) along thruster centerline at 1 m distance from a retarding potential analyzer. At 10 V$_e$, the electrodes only increase the ion energy by ~3 V, but at 30 V$_e$ the energy is increased by 19 – 25 V. The different energy behavior is also a goal of the in-channel measurements.
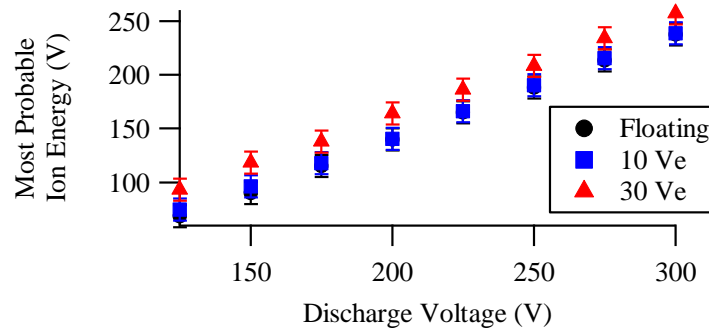
American Institute of Aeronautics and Astronautics

Figure 10. Most probable ion energy for Floating, 10 V_e, and 30 V_e at 9 A. The small change in ion energy at 10 V_e and large change at 30 V_e is present at all voltages tested.

The electrodes caused changes in the in-channel potential contours. There are two main proposed causes of these changes the cusp-magnetic field, and a shift of primary anode. As mentioned before, the thermalized potential assumption makes the magnetic field lines become equipotential lines to the first order. The higher bias cases seem to support this as the high potential domed regions conform to the cusp field lines. The second cause is a shift in the discharge current collection. Figure 11 shows the current collected by the electrodes at 10 and 30 V_e. The total current is 9 A, thus at 10 V_e the electrodes take ~22% of the discharge current, but at 30 V_e almost all of the current is on the electrodes. As the electrodes are biased off the anode line, there is current cycling thus the anode is never at zero current. This means that at 30 V_e the electrodes collect the discharge current and become the dominant anode, or positive terminal. The electrodes then dictate the plasma behavior such as potential fields. This also explains the different ion energy changes between the two electrode biases.
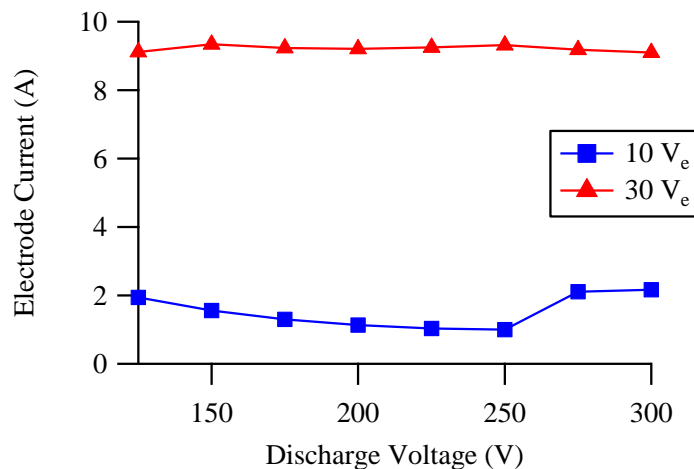

Figure 11. Electrode current at 9 A for 10 V_e and 30 V_e electrode bias. The electrodes draw in almost all of the current at 30 V_e.

A. Acceleration Region

The increased potential range within the discharge channel is largely due to increased maximum potential. At the downstream end of the measured region, the minimum potential is relatively constant around 70 V. Likewise in the far-field the plasma potential is very similar between the three electrode conditions. The largest increase is 0.78 V from Floating to 30 V_e. The increase in maximum potential near the anode without a similar increase in minimum potential results in an increased potential drop and slope. Figure 12 shows the centerline plasma potential measured with the miniature emissive probe from the near anode region to multiple channel lengths downstream. The Floating and 10 V_e cases have nearly identical potential profiles while the 30 V_e profile shows increased maximum potential, but similar far-field potential. This creates a potential profile with a larger gradient.

13
American Institute of Aeronautics and Astronautics

One effect of the sharper potential drop at 30 V_e is a shorter acceleration region. The acceleration region is the axial length where the majority of the potential drop occurs and ions are accelerated by the electric field. The acceleration region can be determined from the plasma potential or electric field. Looking at the centerline plasma potential shown in Figure 12, the acceleration region is taken to be between 90% and 10% of the total potential drop. From the electric field profile shown in Figure 13, which is simply the derivative of the potential, the acceleration region is taken to be between 0.15 E_{max} on either side of the peak. Linnell[10] and Reid[6] use the same analysis .
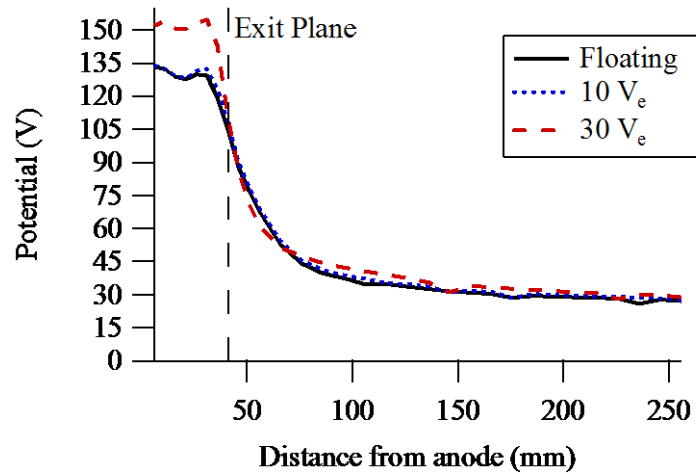

Figure 12. Centerline potential profile for xenon cases tested.
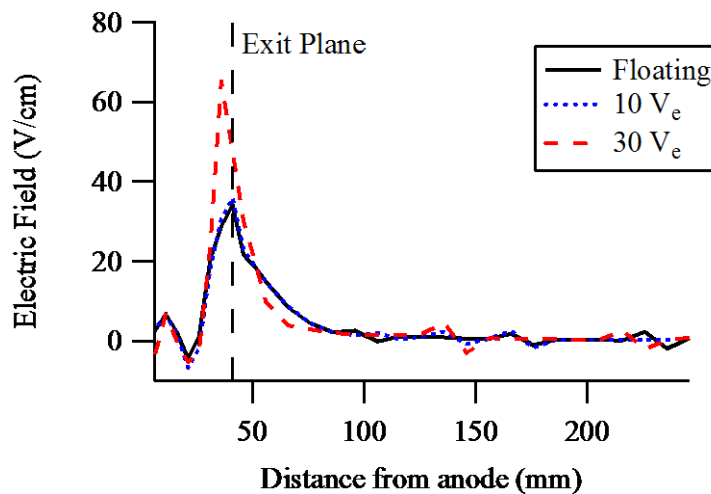

Figure 13. Centerline electric field for Floating, 10, and 30 V_e.

Table 1 shows the acceleration region length calculated with the two methods. The electric field method gives a longer acceleration region. At 30 V_e though, the two methods give very different values for the acceleration length, 44.5 vs 32.8 mm. The electric field method predicts a much shorter acceleration region. This is due to the high maximum electric field at 30 V_e which causes the 0.15 E_{max} value to be larger and results in a smaller range. If we use the 0.15 E_{max} value from 10 V_e, the acceleration length at 30 V_e becomes 41 mm, which is closer to the potential calculated length of 44.46 mm. Whichever method is used, the acceleration region shrinks with increased electrode potential especially at the higher electrode voltage.

American Institute of Aeronautics and Astronautics

Table 1. Acceleration region locations as distance from the anode measured along channel centerline for Floating, 10 and 30 V$_e$.

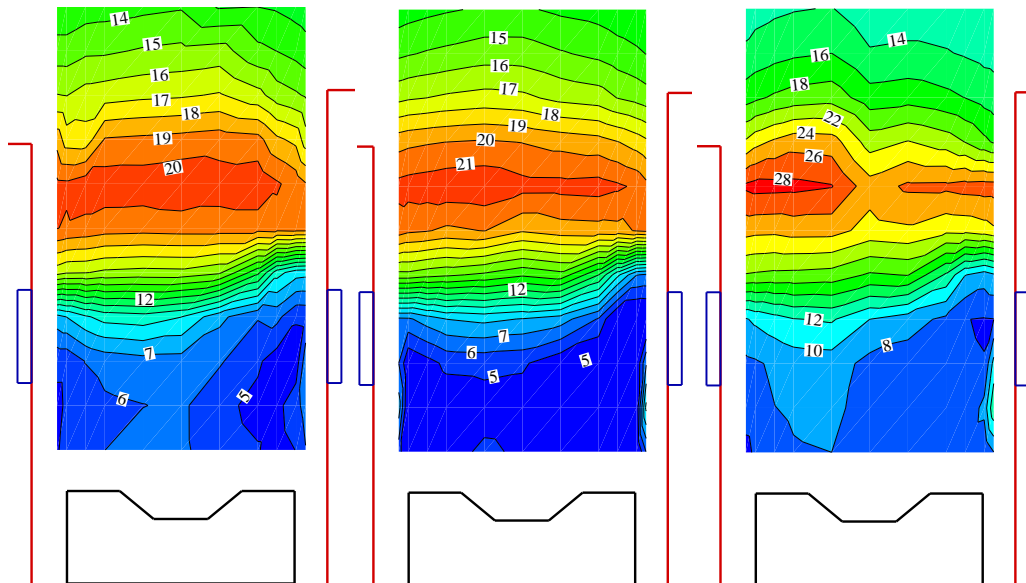|	Floating	10 V$_e$	30 V$_e$
Potential			
Accel Start (mm)	34.01	35.87	36.38
Accel End (mm)	82.59	83.83	80.84
Accel Length (mm)	48.59	47.96	44.46
Electric Field			
Accel Start (mm)	32.03	32.81	33.37
Accel End (mm)	84.30	83.78	66.17
Accel Length (mm)	52.26	50.98	32.80

B. Electron Temperature

The electron temperature is obtained from the floating and plasma potential from the emissive probe according to Eq. (21), where V_f is the floating potential, k_B is the Boltzmann constant, e is the electron charge, and m_e and m_i are the electron and ion masses, respectively.[6, 10]

$$V_p - V_f = -\frac{k_B T_e}{e} ln\left(0.605\sqrt{\frac{2\pi m_e}{m_i}}\right) \tag{21}$$

Figure 14 shows the calculated electron temperature contours for the three electrode conditions. The contours are not perfectly symmetric with respect to the centerline due to uncertainty in the measurement and due to the fact the HET cannot be truly 2D symmetric due to the annular configuration. For example, the magnetic flux density will be larger at the inner wall than outer wall because of the smaller inner wall area. The electron temperature is highest near the channel exit where the radial magnetic field peak is located. The area of highest temperature is typically associated with the Hall current and the ionization region. The maximum electron temperature increased with electrode bias. From Floating to 10 V$_e$ the temperature increases by only 1 eV, from 20 to 21 eV. This small increase in temperature and thus electron energy indicates very little change occurs in the electron energy distribution.

Figure 14. Electron temperature in the discharge channel for Floating, 10, and 30 V$_e$.

15
American Institute of Aeronautics and Astronautics

A second possible effect of the increased electron temperature is increased electron gyroradius along magnetic field lines. The electron temperature near the electrodes also increases noticeably from Floating to 30 V_e. This causes an increase in the electron thermal velocity. For a constant magnetic field, as done in this work, the increased velocity will increase the Larmor, or gyro radius. An increased gyro radius means the electrons are not as well magnetized and trapped by the magnetic field lines, thus an increase in the cross-field mobility and electron current is possible. Comparing the gyroradius near the electrodes for a 7 eV electron (Floating) to 10 eV (30 V_e), the gyroradius increases from 0.25 mm to 0.3 mm assuming a 250 G magnetic field. This increase is small, but may play a minor role in the high electron current seen at high electrode bias. One method to avoid the increase in high current would be to increase the cusp-magnetic field strength.

C. Near-wall Sheath

An area of interest of this work with in-channel electrodes and their shielding cusp fields is the interaction of the magnetic field with the near-wall plasma sheath. The plasma sheath is a thin region of plasma the surrounds any surface exposed to the plasma whether it be insulating or conducting. For the positively biased electrode in this work, the sheath formed is typically an electron repelling sheath. The sheath size is controlled by the balance between the electron flux to the conducting surface, and the current draw necessary to maintain the discharge. In most cases, the electron flux is higher than necessary for the discharge, thus an electron repelling sheath develops to reduce the flux. It is also possible to have an electron attracting sheath if the thermal flux is insufficient to maintain the discharge current. This situation is present in cases of electrodes with surface areas too small for sufficient flux.[15,16]

Another method to control the electron flux to electrodes is with magnetic fields, specifically fields parallel or at small angles to the electrodes. The cusp fields that surround the wall electrodes in this work are one such example. The presence of strong magnetic fields can magnetize electrons, reducing their mobility and flux toward the electrode. This in effect performs the function of an electron repelling sheath, and can reduce or remove the sheath thickness. Magnetization of electrons occurs if the electron Hall parameter squared, Ω_e^2, is much larger than unity. The Hall parameter squared at a distance 3 mm from the electrodes, approximately where the closest probe point is taken, is 164, which means the electrons are magnetized. This leads to the conclusion that the sheath should be strongly affected by the cusp magnetic field. However the domed contours only appear at 10 and 30 V_e. The electrodes thus also play an important role in the contour shaping and sheath changes.

The magnetization of the electron causes a reduction of electron flux to the electrodes as desired. This can be seen from a plot of cusp magnet current versus the electrode current as shown in Figure 15. The thruster was run at 175 V, 9 A discharge and 10 V_e. The inner and outer cusp magnet currents were varied at the same time to maintain symmetry. For the results presented here, the cusp magnets were held constant at 15 A. This behavior suggests that the sheath shrinks in size as the electron flux to the electrodes is reduced by the magnetic fields. This causes the main anode to have increased current, thereby shifting dominance to the anode. Stronger cusp fields may be able to reduce the electrode current at 30 V_e and give future T/P improvements.

It was also observed that an increase in one cusp magnet, the inner or outer, and cause a drop in the associated electrode current, and increase in the other. For example, an increase in the inner cusp magnet strength decreases the inner electrode current but increases the outer electrode current. However, the total electrode current remained nominally constant. The mass flow and discharge voltage are held constant, thus the shifting of currents is due to changing magnetization of electrons around one electrode, causing the other electrode to draw more current to maintain the discharge. This would mean the inner and outer electrode sheaths grow and shrink in a dependant fashion, which is logical given their power supplies have the same negative connection. The electrode behavior indicates that the cusp magnetic fields are having a significant effect on the electron flux and sheath properties. Further investigation is needed to better quantify the interactions.
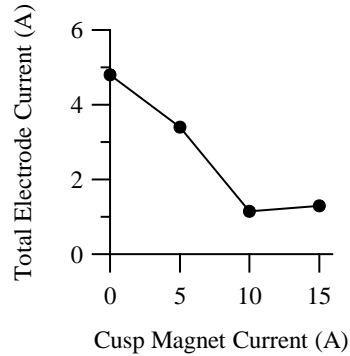
Figure 15. Total electrode current (for both electrodes) as function of the cusp magnet current. The thruster was operated at 175 V, 9 A discharge with 10 V_e electrodes. Both cusp magnets had the same current. For reference, the cusp magnets were at 15 A for all the in-channel measurements.

VI.   Conclusion

This paper presents a continuing investigation of a ion-focusing HET that uses in-channel electrodes. Previous efforts have shown the electrodes increase the performance across the metrics of thrust, T/P, specific impulse, and anode efficiency. Plume measurements also show a reduction in the plume divergence angle, an increase in propellant efficiency, and an increase in ion energy. The in-channel measurements presented here show the electrodes in conjunction with the cusp-magnetic fields create domed-shaped high-potential contours around the electrodes. These domed contours generate focusing electric fields and thus reduce the plume angle and increase thrust. The differences in ion energy between the two electrode bias levels are attributed to a shift of the discharge current from the main anode/propellant distributor to the electrodes. At 30 V_e, the electrodes become the dominant positive terminal and thus dictate plasma behavior. In addition comparison of BN and graphite material showed little change, which indicates the change in SEE with the addition of graphite has little effect at these discharge conditions. The shifting current between the two electrodes with changing cusp magnetic field strength indicates changing electron magnetization and sheath behavior.

Acknowledgments

References

[1]   Zhurin, V. V., Kaufman, H. R., and Robinson, R. S. "Physics of Closed Drift Thrusters," *Plasma Sources Science and Technology* Vol. 8, No. 1, 1999, pp. R1-R20.

[2]   Hofer, R. R. "Development and Characterization of High-Efficiency, High-Specific Impulse Xenon Hall Thrusters," *Aerospace Engineering*. Ph.D. Dissertation, University of Michigan, Ann Arbor, MI, 2004.

[3]   Xu, K. G., and Walker, M. L. R. "Plume Characterization of an Ion Focusing Hall Thruster," *47th AIAA Joint Propulsion Conference*. AIAA-2011-5588, San Diego, CA, 2011.

[4]   McVey, J. B., Britt, E. J., Engelman, S. F., Gulczinski, F. S., Beiting, E. J., and Pollard, J. E. "Characteristics of the T-220HT Hall-Effect Thruster," *39th Joint Propulsion Conference*. AIAA 2003-5158, Huntsville, AL, 2003.

[5]   Haas, J. M. "Low-Perturbation Interrogation of the Internal and Near-Field Plasma Structure of a Hall Thruster Using a High-Speed Probe Positioning System," *Aerospace Engineering*. Ph.D. Dissertation, University of Michigan, Ann Arbor, MI, 2001.

[6]   Reid, B. M. "The Influence of Neutral Flow Rate in the Operation of Hall Thrusters," *Aerospace Engineering*. Ph.D., University of Michigan, 2009.

[7]   Mikellides, I. G., Katz, I., Hofer, R. R., and Goebel, D. M. "Magnetic Shielding of the Acceleration Channel Walls in a Long-Life Hall Thruster," *46th AIAA Joint Propulsion Conference*. AIAA-2010-6942, Nashville, TN, 2010.

[8]   Shastry, R. "Experimental Characterization of the Near-Wall Region in Hall Thrusters and its Implications on Performance and Lifetime," *Aerospace Engineering*. Ph.D., University of Michigan, 2011.

[9]   Goebel, D. M., and Katz, I. *Fundamentals of Electric Propulsion: Ion and Hall Thrusters*. Pasadena: Jet Propulsion Laboratory, 2008.

[10]   Linnell, J. A. "An Evaluation of Krypton Propellant in Hall Thrusters," *Aerospace Engineering*. Ph.D., University of Michigan, 2007.

[11]   Hofer, R. R., Mikellides, I. G., Katz, I., and Goebel, D. M. "Wall Sheath and Electron Mobility Modeling in Hybrid-PIC Hall Thruster Simulations," *43rd AIAA Joint Propulsion Conference*. AIAA-2007-5267, Cincinnati, OH, 2007.

[12]   Allis, M. K., Gascon, N., Vialard-Goudou, C., and Cappelli, M. A. "A Comparison of s-D Hybrid Hall Thruster Model to Experimental Measurements," *40th AIAA Joint Propulsion Conference*. AIAA-2004-3951, Fort Lauderdale, FL, 2004.

[13]   Huang, W., and Gallimore, A. "Neutral Flow Evolution in a Six-Kilowatt Hall Thruster," *Journal of Propulsion and Power* Vol. 27, No. 3, 2011, pp. 553-563.

[14]   Mitchner, M., and Kruger, C. H. J. *Partially Ionized Gases*: John Wiley & Sons Inc, 1973.

[15]   Dorf, L., Raitses, Y., and Fisch, N. J. "Experimental Studies of Anode Sheath Phenomena in a Hall Thruster Discharge," *Journal of Applied Physics* Vol. 97, 2005.

[16]   Anders, A., and Anders, S. "The Working Principle of the Hollow-Anode Plasma Source," *Plasma Sources Science and Technology* Vol. 4, 1995, pp. 571-575.